Effects of autoionization in electron loss from heliumlike highly charged ions in fast collisions with atomic particles

K. N. Lyashchenko,[1,*] O. Yu. Andreev,[1] and A. B. Voitkiv[2]

[1]*Department of Physics, St. Petersburg State University, 7/9 Universitetskaya Naberezhnaya, St. Petersburg 199034, Russia*

[2]*Institute for Theoretical Physics I, Heinrich-Heine-University of Düsseldorf, Düsseldorf 40225, Germany*

(Received 3 July 2017; published 8 November 2017)

We study theoretically single-electron loss from the ground state of a heliumlike highly charged ion in fast collisions with an atomic particle (a nucleus or an atom), focusing on electron emission energies where the so-called excitation-autoionization channel of electron loss becomes of importance. The presence of this channel leads to the appearance of sharp structures in the energy distribution of the emitted electrons and may also noticeably influence the angular distributions of the emission in the vicinity of autoionization resonances. We performed calculations for electron loss from $Ca^{18+}(1s^2)$ and $Zn^{28+}(1s^2)$ in 100 MeV/u collisions with neon. It is shown that two qualitatively different subchannels (which involve either one or two interactions between the electrons of the ion and the incident atomic particle) substantially contribute to excitation-autoionization and take active part in the interference with the direct channel of electron loss; however, they practically do not interfere with each other. Our consideration also shows that the account of QED corrections is important for an accurate description of electron loss even from relatively light heliumlike HCIs.

DOI: 10.1103/PhysRevA.96.052702

I. INTRODUCTION

Atomic systems with more than one electron possess states which can spontaneously decay, emitting an electron. They are called autoionizing states and can be highly visible in many atomic processes, e.g., photo ionization and ionization by electron impact. In particular, this is especially the case when the energy transfer to the system is close to the difference between the energies of an autoionizing state and the initial state of the system. Under such circumstances, the initial system can undergo a transition to the continuum not only directly but also via excitation to the autoionizing state with its consequent Auger decay (the so-called excitation-autoionization, EA, channel).

The role of autoionization has been extensively studied for electron-ion and electron-atom collisions. A large number of atomic systems was considered. They include, for instance, helium and heliumlike lithium (see, e.g., Refs. [1–4]); various ions: Mg^+, Ca^+, Sr^+ [5], Ga^+ [6], Ba^+ [5,7,8], C^{3+}, N^{3+}, O^{3+} [9], Ti^{3+}, Zr^{3+}, and Hf^{3+} [10], Sn^{q+} ($q = 4$–13) [11], Xe^{q+} ($q = -6,10$)1 [12,13]; light lithiumlike ions ranging from B^{2+} to F^{6+} [14,15]; and excited C^+ ions [16]. It was, in particular, found that the EA channel and its interference with the direct channel can be of great importance in the processes of electron impact ionization and electron loss.

New features arise in the electron loss process when it occurs from highly charged ions where relativistic and QED effects may be of importance. Calculations for electron loss from lithiumlike highly charged Ar^{15+}, Fe^{23+}, Kr^{33+}, and Xe^{51+} ions by electron impact were performed in Ref. [17]. According to the results reported in Ref. [17], the Breit interaction as well as the $M2$ transitions may substantially influence the EA channel and the total electron loss. The cross section for electron loss from berylliumlike highly charged ions (HCIs) in collisions with bare atomic nuclei, differential in the emission angle, was calculated in Ref. [18], where a significant influence of the Breit interaction on the EA channel was predicted.

A review on the various aspects of autoionization in electron-ion collisions can be found in Ref. [19].

In the present paper, we shall consider single-electron loss from heliumlike HCIs occurring in collisions with atomic particles (atoms, nuclei). The collisions are supposed to be fast enough such that the interaction between the electrons of the ion and the atomic particle remains much weaker than the interaction of these electrons with the nucleus of the ion and therefore can be treated as perturbation. The main focus of our study is on the role of autoionization in this process, which can be significant when the energy of the emitted electron is close to the difference between the energy of an autoionizing state of a heliumlike HCI and the energy of the final state of the residual hydrogenlike ion. In such a case, the autoionizing state can participate in the process via the corresponding EA channel. This is illustrated in Fig. 1, where both the direct and EA channels of electron loss are schematically depicted.

The topic considered in the present paper is of interest because of the following reasons. First, to our knowledge, although compared to helium and low-charged heliumlike ions, heliumlike HCIs possess important and interesting features, the role of autoionization in electron loss from the latter has not yet been studied. Second, if the electron loss proceeds from the ground state of the ion then the interaction between the electrons of the ion (electron correlations in a strong field) are expected to play an especially prominent role in the EA channel. Third, we are not aware about studies of autoionization in electron loss which is triggered by fast collisions with neutral atoms. Therefore, the results presented in this paper not only fill a substantial gap in the theoretical studies of autoionization but also can serve as a guide for future experimental activities in this field.

Below we suppose that the HCI is initially in its ground state ($1s^2$). Under such a condition there are two main ways to excite an autoionizing state of the HCI. In the first of them, the

*laywer92@mail.ru

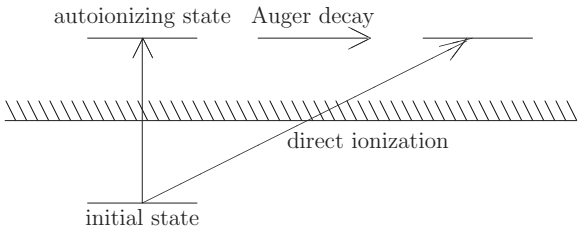

FIG. 1. Electron loss from HCI via the direct channel and the EA channel.

incident particle interacts with only one of the two electrons of the HCI. We note that this way of populating an autoionizing state is not possible without the interaction between the electrons of the HCI. In the other one, the excitation of the autoionizing state proceeds via the interaction of the incident particle with both electrons of the HCI.

Unlike the EA, the direct channel of electron loss represents essentially one-electron process in which the "passive" electron is merely a spectator.

The relativistic units ($\hbar = c = m_e = 1$) are used throughout unless otherwise stated.

II. GENERAL CONSIDERATION

Our description of a free heliumlike HCI is based on the line-profile approach (LPA) [20,21] of QED. The Furry picture is used, in which the Coulomb interaction of the electrons of the HCI with its nucleus is fully taken into account from the onset. The Dirac equation is employed to treat both bound electrons and the emitted electron. The interaction of these electrons with the quantized electromagnetic and electron-positron fields is treated according to the standard QED perturbation theory. This interaction is taken into account in the zeroth and first orders of the perturbation expansion. Besides, the leading parts of the higher order corrections in the electron-electron interaction are also included into the treatment according to the LPA [20].

Since the interaction of the electrons with the field of the incident atomic particle is assumed to be relatively weak, it will be treated using the lowest possible orders of relativistic perturbation theory. As was already mentioned, the direct channel of electron loss is essentially a one-electron process. Therefore, for its description, it suffices to use the first order of perturbation theory in the interaction with the incident atomic particle.

The situation with the treatment of the EA channel of electron loss is somewhat more complicated. Indeed, it was noted in the introduction that this channel involves two qualitatively different pathways in which the incident atomic particle interacts either with only one of the two electrons (the EA_1 subchannel) or with each of them (the EA_2 subchannel). Therefore, the description of the EA_2 necessitates the second order of the perturbation theory whereas for the EA_1 subchannel it is sufficient to use just the first order.

In Fig. 2 we illustrate our description of electron loss from the ground state by the impact of an atomic particle by showing Feynman graphs which correspond to the first and second orders of the perturbation theory with respect to the interaction

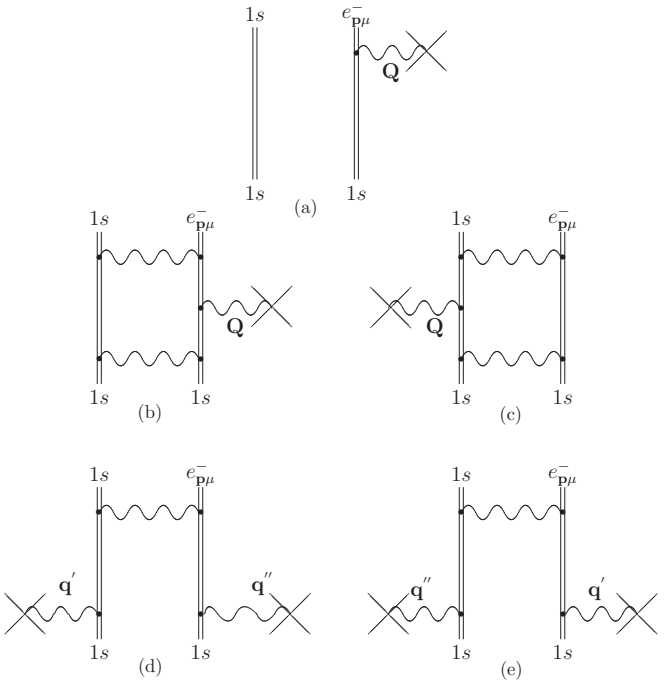

FIG. 2. Feynman graphs for electron loss from the ground state of a heliumlike HCI. (a) The leading (in the electron-electron interaction) contribution to the direct channel. [(b), (c)] The leading contributions to the EA_1 subchannel. [(d), (e)] The leading contributions to the EA_2 subchannel. The vectors $\mathbf{Q}$, $\mathbf{q}'$, and $\mathbf{q}''$ denote the momentums transferred by the external field to the HCI ($\mathbf{q}' + \mathbf{q}'' = \mathbf{Q}$).

between the electrons of the HCI and the field of the atomic particle. We note that for each channel of the electron loss the corresponding graphs depict just the respective leading contributions in the electron-electron interaction and that in our calculations we take into account also various corrections to them.

Figure 2(a) represents the main contribution to the direct channel of electron loss in which one of the electrons of the ion, via absorbtion of a virtual photon, makes a transition to the continuum, whereas the other electron remains merely a spectator. Figures 2(b)–2(e) include leading contributions to the EA channel [22].

A. Construction of two-electron states of a free HCI

In the framework of the LPA, the initial and final states of a free HCI in the zeroth-order of QED perturbation theory are chosen as configurations of noninteracting electrons in the j-j coupling scheme. The interaction with the quantized fields leads to various corrections to these states. They are given as linear combinations of many different configurations of the noninteracting electrons in the j-j scheme. The coefficients in these linear combinations (the mixing coefficients) are obtained in the framework of the LPA.

By employing the rest frame of the HCI, taking the position of the HCI's nucleus as the origin, and denoting by $\mathbf{r}_1$ and $\mathbf{r}_2$ the coordinates of the electrons of the HCI, we give the two-electron wave functions in the zeroth order of perturbation

theory by

$$\Psi^{(0)}_{JMn_1j_1l_1n_2j_2l_2}(\mathbf{r}_1,\mathbf{r}_2) = N\sum_{m_1,m_2} C^{j_1,j_2}_{JM}(m_1,m_2) \times \det\{\psi_{n_1j_1l_1m_1}(\mathbf{r}_1)\psi_{n_2j_2l_2m_2}(\mathbf{r}_2)\}. \quad (1)$$

Here, N is the normalization constant (equal to $1/2$ for equivalent electrons and to $1/\sqrt{2}$ otherwise), $C^{j_1,j_2}_{JM}(m_1,m_2)$ are the Clebsch-Gordan coefficients, ψ_{n_i,j_i,l_i,m_i} is a solution of the one-electron Dirac equation where n_i is the principal quantum number, j_i is the total angular momentum, m_i is its projection, and l_i defines parity $[(-1)^{l_i}]$, where the index i ($i = 1, 2$) labels the ith electron of the HCI.

The emitted electron with momentum $\mathbf{p}$, energy $\epsilon_p = \sqrt{1+p^2}$, and polarization μ is described by the following expansion [23]:

$$\psi_{\boldsymbol{p},\mu}(\boldsymbol{r}) = \int d\varepsilon \sum_{jlm} a_{\boldsymbol{p}\mu,\varepsilon jlm}\psi_{\varepsilon jlm}(\boldsymbol{r}), \quad (2)$$

where

$$a_{\boldsymbol{p}\mu,\varepsilon jlm} = \frac{(2\pi)^{3/2}}{\sqrt{p\epsilon_p}} i^l e^{-i\phi_{jl}} [\Omega^{+}_{jlm}(\boldsymbol{p}),\upsilon_\mu(\boldsymbol{p})]\delta(\epsilon_p - \varepsilon). \quad (3)$$

In Eq. (3), the ϕ_{jl} is the Coulomb phase shift, $\Omega_{jlm}(\boldsymbol{p})$ is the spherical spinor, and $\upsilon_\mu(\boldsymbol{p})$ is the spinor with projection $\mu = \pm 1/2$ on the electron momentum ($\boldsymbol{p}$)

$$\frac{\boldsymbol{p}\,\hat{\boldsymbol{\sigma}}}{2p}\upsilon_\mu(\boldsymbol{p}) = \mu\upsilon_\mu(\boldsymbol{p}), \quad (4)$$

where $\hat{\boldsymbol{\sigma}}$ is the Pauli vector. It is convenient to describe the final two-electron state $(1s, e^-)$, which contains the emitted electron, as a linear combination of the following determinants:

$$\frac{1}{\sqrt{2}}\det\{\psi_{n_bj_bl_bm_b}(\mathbf{r}_1)\psi_{\boldsymbol{p},\mu}(\mathbf{r}_2)\} = \sum_{JMjlm} C^{j_b,j}_{JM}(m_b,\mu)\int d\varepsilon\, a_{\boldsymbol{p}\mu,\varepsilon jlm}\Psi^{(0)}_{JMn_bj_bl_b\varepsilon jl}(\mathbf{r}_1,\mathbf{r}_2), \quad (5)$$

where the quantum numbers n_b, j_b, l_b, and m_b refer to the $1s$ electron in the resudial hydrogenlike HCI.

In order to take into account the QED corrections such as the interelectron interaction correction, the electron self-energy, and the vacuum polarization corrections, we employ the LPA. According to the LPA, we construct new functions, which are given by [20]

$$\Phi_m(\boldsymbol{r}_1,\boldsymbol{r}_2) = \sum_{k\in g} B_{km}\Psi^{(0)}_k(\boldsymbol{r}_1,\boldsymbol{r}_2) + \sum_{n\notin g, l\in g}[\Delta V]_{nl}\frac{B_{lm}}{E^{(0)}_m - E^{(0)}_n}\Psi^{(0)}_n(\boldsymbol{r}_1,\boldsymbol{r}_2), \quad (6)$$

where m, k, l, and n label the two-electron configurations and g denotes the set of all two-electron configurations considered in this work. The set g includes all the two-electron configurations composed of $1s$, $2s$, $2p$, $3s$, $3p$, $3d$, $4s$, $4p$, $4d$, and $4f$ electrons and the electron in the continuum. The ΔV represents the matrix of the QED corrections: the one- and two-photon exchange corrections, the electron self-energy correction, and the vacuum polarization correction.

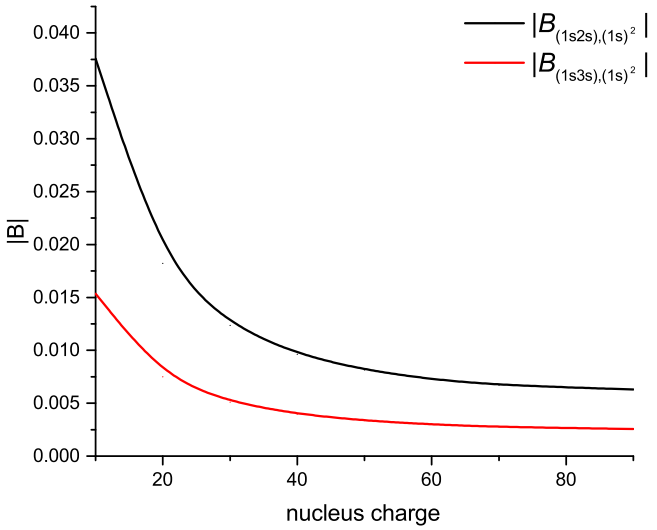

FIG. 3. The absolute values of the mixing coefficients for the two-electron configuration $1s^2$ [see Eq. (7)] given as a function of Z_I. The upper and lower curves refer to $B_{(1s,2s)(1s^2)}$ and $B_{(1s,3s)(1s^2)}$, respectively.

For relatively light heliumlike HCIs, it is necessary to take into account the contribution of the imaginary part of the two-photon exchange correction to the matrix ΔV, which determines the Auger widths. The contribution of the Auger part of the two-photon exchange correction (in particular, the nondiagonal elements, which are very important) was not considered before. Therefore, we discus this point in some detail in the appendix, where the explicit expression for this correction to the matrix ΔV is given.

The first term on the right-hand side in Eq. (6) corresponds to the mixing of the configurations from the set g. The mixing coefficients B_{km} are obtained within the LPA. The second term on the right-hand side in Eq. (6) takes into account all other configurations which are not included in the set g. The two-electron configuration energy in zeroth-order $E^{(0)}_n$ is the sum of the corresponding one-electron Dirac energies.

For example, the ground two-electron state constructed according to Eq. (6) has the following form:

$$\Phi_{(1s^2)} = B_{(1s^2),(1s^2)}\Psi^{(0)}_{(1s^2)} + B_{(1s2s),(1s^2)}\Psi^{(0)}_{(1s2s)} + B_{(1s3s),(1s^2)}\Psi^{(0)}_{(1s3s)} + \cdots, \quad (7)$$

where only the main terms of the first sum in Eq. (6) are explicitly given. In order to describe the EA_1 subchannel of electron loss from the ground state of a HCI, it is necessary to take into account the contributions from the $(1s2s)$ and $(1s3s)$ configurations. The absolute values of the mixing coefficients corresponding to these configurations are shown in Fig. 3, where they are given as a function of the atomic number Z_I of the HCI. It is seen in the figure that the initial rapid decrease in the magnitude of the mixing coefficients at not very large Z_I is then replaced by a much slower decrease at higher Z_I and that these coefficients become almost constants at very high Z_I.

This behavior can be understood by noting that the Coulomb and the Breit parts of the electron-electron interaction scale approximately as $\sim Z_I$ and Z_I^3, respectively. Since the energy

differences, $E_n^{(0)} - E_m^{(0)}$ $(n \neq m)$, scale with Z_I as Z_I^2, the contribution of the Coulomb and Breit parts to the mixing coefficients are proportional to $1/Z_I$ and Z_I, respectively. Therefore, at not very high Z_I, where the Coulomb part of the electron-electron interaction strongly dominates, we observe that the mixing coefficients depend on Z_I as $1/Z_I$, whereas at very high Z_I, where the effective strength of Breit interaction becomes overall comparable to that of the Coulomb one, these coefficients are almost Z_I independent.

To conclude this subsection, we note that the LPA enables one to describe with very good accuracy highly charged ions with a few electrons (see Refs. [20,21] for benchmark LPA calculations). In particular, one of the advantages of the LPA is that within this method one may not only take exactly into account the lowest orders of the standard QED perturbation theory but also account partly for the contributions of all higher orders and implement such calculations with a relative economy of computational resources and time. The application of the LPA, however, has a limiting factor: The computation becomes increasingly cumbersome when the relative role of the electron correlations increases (that makes it necessary to employ very large basis sets). Therefore, the application of the LPA to light systems (like, e.g., He or Li^+) would either yield inaccurate results or demand powerful computers and be very time-consuming.

B. Electron loss in collisions with a bare atomic nucleus

It is convenient to give the basic consideration of electron loss in fast collisions with atomic particle using the rest frame of the HCI. We take the position of the HCI's nucleus as the origin and denote by $\mathbf{r}_1$ and $\mathbf{r}_2$ the coordinates of the electrons of the HCI. We shall suppose that the energy of the incident particle is so high that its change in the process is negligible compared to its initial value. This allows us to describe the particle as moving along a straight-line classical trajectory $\mathbf{R}(t) = (\mathbf{b}, vt)$, where $\mathbf{b} = (b_x, b_y)$ is the impact parameter, $\mathbf{v} = (0,0,v)$ is the velocity of the particle, and t denotes the time.

The field of the particle represents a relatively weak perturbation for the electrons of the HCI provided the charge (the atomic number) Z_A of the particle and the collision velocity v satisfy the condition $\frac{\alpha Z_A}{v} \ll 1$, where α is the fine-structure constant. Below we suppose that this condition is fulfilled which enables one to restrict our consideration just to the first and second orders of the perturbation theory in the interaction between the electrons and the incident particle.

In this subsection, we assume that the particle is a bare atomic nucleus. Then, within the first order of the perturbation theory, the amplitude of electron loss from the HCI is given by

$$A_{if}^{(1)}(\mathbf{b}) = -i \int_{-\infty}^{\infty} dt\, \langle \Phi_f | W_{\mathbf{b}}(\mathbf{r}_1,t) + W_{\mathbf{b}}(\mathbf{r}_2,t) | \Phi_i \rangle e^{it(E_f^{(0)} - E_i^{(0)})}, \tag{8}$$

$$W_{\mathbf{b}}(\mathbf{r}_i,t) = -\frac{\gamma Z_A \alpha (1 - v\alpha_z)}{\sqrt{(\mathbf{b} - \mathbf{r}_{i,\perp})^2 + \gamma^2 (vt - r_{i,z})^2}}, \tag{9}$$

where $W_{\mathbf{b}}(\mathbf{r}_i,t)$ is the interaction between the atomic particle and the ith ionic electron ($i = 1,2$). In Eq. (9), $\gamma = 1/\sqrt{1 - v^2}$ is the Lorentz factor of the collision and α_z is the corresponding Dirac α matrix. In Eq. (8) and below, the indices i and f denote the initial ($1s^2$) and final ($1s_{m_b}, e^-_{\mathbf{p}\mu}$) states, respectively, where m_b and μ are polarizations of the corresponding electrons in the final state.

It is convenient to work with the transition amplitude in the momentum space, which is obtained from Eq. (8) by performing the Fourier transformation

$$S_{if}^{(1)}(\mathbf{Q}_\perp) = \frac{1}{2\pi} \int d^2\mathbf{b}\, A_{if}^{(1)}(\mathbf{b}) e^{i\mathbf{Q}_\perp \mathbf{b}}, \tag{10}$$

which results in

$$S_{if}^{(1)}(\mathbf{Q}_\perp) = 2i \frac{Z_A \alpha}{v} \frac{\langle \Phi_f | W_{\mathbf{Q}_\perp}(\mathbf{r_1}) + W_{\mathbf{Q}_\perp}(\mathbf{r_2}) | \Phi_i \rangle}{Q_\perp^2 + \frac{Q_{\min}^2}{\gamma^2}}, \tag{11}$$

where

$$W_{\mathbf{Q}_\perp}(\mathbf{r}_i) = e^{i\mathbf{Q}\mathbf{r}_i}(1 - v\alpha_z). \tag{12}$$

In the above expressions, the momentum transfer $\mathbf{Q}$ to the HCI in the collision reads

$$\mathbf{Q} = (\mathbf{Q}_\perp, Q_{\min}), \quad Q_{\min} = \frac{E_f^{(0)} - E_i^{(0)}}{v}, \tag{13}$$

where $E_i^{(0)}$ is the energy of the initial state of the HCI and $E_f^{(0)}$ is the sum of the energies of the emitted electron and the residual hydrogenlike ion.

The second-order contribution to the amplitude of electron loss from the HCI reads

$$A_{if}^{(2)}(\mathbf{b}) = (-i)^2 \sum_m \int_{-\infty}^{\infty} dt\, \langle \Phi_f | W_{\mathbf{b}}(\mathbf{r}_1,t) + W_{\mathbf{b}}(\mathbf{r}_2,t) \big| \Psi_m^{(0)} \rangle e^{it(E_f^{(0)} - E_m^{(0)})} \times \int_{-\infty}^{t} dt' \langle \Psi_m^{(0)} \big| W_{\mathbf{b}}(\mathbf{r}_1,t') + W_{\mathbf{b}}(\mathbf{r}_2,t') | \Phi_i \rangle e^{it'(E_m^{(0)} - E_i^{(0)})}, \tag{14}$$

where the summation is performed over the complete basis set of two-electron wave functions $\Psi_m^{(0)}$ with corresponding energies $E_m^{(0)}$. Like in the first-order consideration described above, we perform the Fourier transformation to obtain the following result:

$$S_{if}^{(2)}(\mathbf{Q}_\perp) = \sum_m \int dq_z \frac{1}{q_z - \frac{E_f^{(0)} - E_m^{(0)}}{v} - i0} f_m(q_z), \tag{15}$$

where

$$f_m(q_z) = -i \left(\frac{Z_A \alpha}{v\pi} \right)^2 \int d^2\mathbf{q}_\perp \frac{\langle \Phi_f | W_{\mathbf{q}_\perp}(\mathbf{r}_1) + W_{\mathbf{q}_\perp}(\mathbf{r}_2) \big| \Psi_m^{(0)} \rangle}{q_\perp^2 + \frac{q_z^2}{\gamma^2}} \frac{\langle \Psi_m^{(0)} \big| W_{\mathbf{Q}-\mathbf{q}_\perp}(\mathbf{r}_1) + W_{\mathbf{Q}-\mathbf{q}_\perp}(\mathbf{r}_2) | \Phi_i \rangle}{(\mathbf{Q}_\perp - \mathbf{q}_\perp)^2 + \frac{(Q_{\min} - q_z)^2}{\gamma^2}}. \tag{16}$$

Performing the Sokhotski-Plemelj theorem for the q_z integral in Eq. (15), we can rewrite it as follows:

$$S_{if}^{(2)}(\mathbf{Q}_\perp) = \sum_m i\pi f_m\left(\frac{E_f^{(0)} - E_m^{(0)}}{v}\right) + \sum_m \mathrm{P}\int dq_z \frac{1}{q_z - \frac{E_f^{(0)} - E_m^{(0)}}{v}} f_m(q_z), \quad (17)$$

where P denotes the principal value integral.

The fully differential cross section for electron loss by particle impact is given by

$$\frac{d\sigma}{d\epsilon_p d\Omega\, d\mathbf{Q}_\perp} = \frac{\epsilon_p p}{(2\pi)^3}\left|S_{if}^{(1)}(\mathbf{Q}_\perp) + S_{if}^{(2)}(\mathbf{Q}_\perp)\right|^2. \quad (18)$$

It is convenient to split the total contribution to the electron loss into the resonant and nonresonant parts. The nonresonant part amounts to the direct channel of the electron loss, whereas the EA channel represents the resonant part in which the EA_1 and EA_2 subchannels are described by the terms in Eqs. (8) and (14), respectively, containing the corresponding autoionizing states. We note that whereas the splitting into the resonant and nonresonant parts in each order of perturbation theory is strictly speaking not unambiguous and may depend on the approach used, the full calculation for the cross section has a well-defined physical meaning.

C. Electron loss in collisions with a neutral atom

When an ion collides with a neutral atom, the interaction between the electrons of the ion both with the nucleus of the atom and the electrons of the atom can contribute to electron loss from the ion. According to the consideration of first order in the interaction between the ion and atom, the role of the atomic electrons in the electron loss is twofold.

First, in collisions in which the atom remains in its initial internal state (elastic atomic mode), the electrons of the atom tend to screen (fully or partially) the charge of the atomic nucleus (see, e.g., Refs. [24–26]). The screening effect reduces the probability for electrons of the ion to undergo a transition compared to collisions with the corresponding bare atomic nucleus. Second, in collisions, which are inelastic also for the atom, only the interaction with the electrons of the atom may contribute to transitions of the ionic electrons (see, e.g., Refs. [24–26]). In this case, the presence of the atomic electrons increases the probability for the electrons of the ion to make a transition [27].

In collisions, which are characterized by momentum transfers to the atom substantially exceeding typical orbiting momenta of the atomic electrons, the contributions of the elastic and inelastic atomic modes to the cross sections for excitation of (electron loss from) the ion roughly scale as $\sim Z_A^2$ and $\sim Z_A$, respectively, where Z_A is the atomic number of the atom (see, e.g., Ref. [26]). In the present paper, we consider collisions of HCIs with multielectron atoms ($Z_A \gg 1$) only, where the relative contribution of the inelastic mode is small. Therefore, in what follows we shall simply neglect the inelastic atomic mode. For the first order with respect to the interaction of HCI's electrons and incident atom, the contribution from the elastic atomic mode can be obtained from expression Eq. (11)

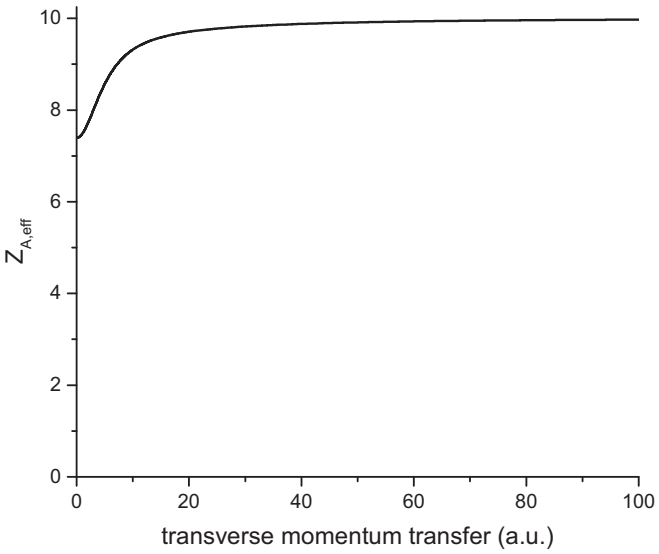

FIG. 4. The effective charge of neon atom as a function of the transverse momentum transfer in collision with $q_{\min} = 4.96$ a.u.

if we replace Z_A by the effective charge of the atom given by [26]

$$Z_{A,\mathrm{eff}} = Z(\mathbf{Q}), \quad (19)$$

where

$$Z(\mathbf{Q}) = Z_A\left(Q_\perp^2 + \frac{Q_{\min}^2}{\gamma^2}\right)\sum_{i=1}^{3}\frac{A_i}{k_i^2 + Q_\perp^2 + \frac{Q_{\min}^2}{\gamma^2}}. \quad (20)$$

The parameters A_i and k_i ($i = 1,2,3$) are tabulated for various atoms in Refs. [28,29] and in the case of a neon atom are equal to

$$A_1 = 0.0188, \quad A_2 = 0.9812, \quad A_3 = 0, \quad (21)$$
$$k_1 = 34.999\,\text{a.u.}, \quad k_2 = 2.566\,\text{a.u.}, \quad k_3 = 0.$$

Figure 4 shows the effective charge of the Ne atom, as a function of the transverse momentum transfer, for electron loss from $Ca^{18+}(1s^2)$ in collisions at an impact energy of 100 MeV/u.

We do the same procedure for the second-order contribution and replace Z_A^2 in Eq. (16) by $Z(\mathbf{q})Z(\mathbf{Q}-\mathbf{q})$.

III. RESULTS AND DISCUSSION

In this section, we present results of our numerical computation for the electron loss cross sections averaged over polarizations of the emitted electron and the bound electron in the final state.

A. Electron loss in the rest frame of the HCI

The process of electron loss looks most simple in the rest frame of the HCI. Therefore, we first consider electron loss in this frame assuming that the incident particle moves along the Z axis (from which the polar angle for the emitted electron is counted).

Figures 5 and 6 show results of our calculations for electron loss from $Ca^{18+}(1s^2)$ in collisions with bare neon nuclei

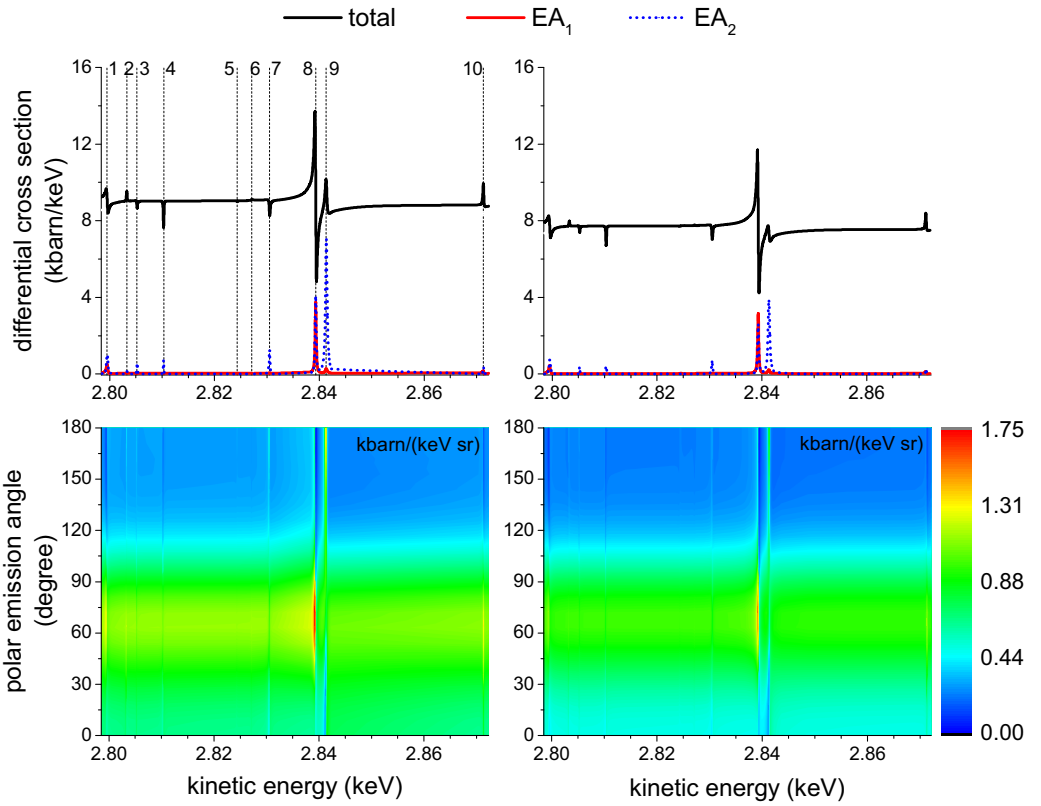

FIG. 5. Cross sections for single electron loss from Ca^{18+} $(1s^2)$ by the impact of 100 MeV/u bare neon nucleus (the left column) and 100 MeV/u neon atom (the right column). The upper and lower panels present the energy and energy-angular distributions, respectively, of the emitted electron. The cross sections are given in the rest frame of the HCI. The numbered vertical lines refer to resonances arising due to the autoionizing states listed in Table I.

(the left column) and neutral neon atoms (the right column) at an impact energy of 100 MeV/u corresponding to the collision velocity $v = 0.428$ r.u. ($\gamma = 1.106$). The upper panels in these figures display the loss cross section (singly) differential in the electron emission energy whereas the lower panels present results for the loss cross section differential in emission energy and angle. In Fig. 5, we consider a relatively broad range of emission energies, whereas in Fig. 6 we focus on the energy range where the $(2s\,2p_{3/2})_{J=1}$ and $(2p^2_{3/2})_{J=2}$ autoionizing states actively participate. The $(2s\,2p_{3/2})_{J=1}$ state was chosen because it leads to the strongest resonance. We note also that in this case both the EA_1 and EA_2 subchannels of the EA channel are equally important.

The energy spectra, shown in the upper panels of these figures, display one of characteristic shapes known as Fano profiles [30]. Such a shape arises because of interference between the direct and the EA channels of electron loss.

The upper panels in these figures also show the contributions of the EA_1 (the lower solid curve) and EA_2 (the dotted curve). In general, these subchannels could interfere with each other. However, according to our numerical calculations, the principal value part of the second-order amplitude in Eq. (17), which is responsible for this interference (see, e.g., Ref. [25]), gives a significantly smaller contribution to this amplitude than the first term in Eq. (17). Therefore, it turns out that the interference between the EA_1 and EA_2 subchannels is practically absent.

It is seen in Figs. 5 and 6 that the main feature of the energy spectrum of the emitted electrons is the presence of sharp maxima and minima, which arise due to the EA channel and its interference with the direct channel of electron loss. These maxima and minima, which reveal the participation of LL autoionizing states in the EA process, are embedded in a smooth background appearing because of the direct electron loss channel. Figures 5 and 6 also show that, unlike in the case with the EA_2, not all autoionizing states are involved in the EA_1 subchannel. This can be understood if we remark that the $(1s2s)_{J=0}$ electron configuration is the only singly excited configuration which is present with a significant weight in the "physical" ground state of a heliumlike HCI. Therefore, if the incident particle interacts just once with the HCI, then only those autoionizing states can be noticeably populated which include two-electron configuration(s) with at least one $2s$ electron.

It is obvious that the EA_2, which involves the interaction of the incident atomic particle with both electrons of the HCI, is free of such a restriction and generally all LL autoionizing states can play a noticeable role in this subchannel.

In Fig. 7, we present the doubly differential cross section as a function of the polar angle of the momentum of the emitted electron. The angular dependence was calculated for five resonant emission energies corresponding to the $(2s^2)_{J=0}$, $(2p_{1/2}2p_{3/2})_{J=2}$, $(2s2p_{3/2})_{J=1}$, $(2p^2_{3/2})_{J=2}$, and $(2p^2_{3/2})_{J=0}$ autoionizing states. It follows from the figure that four

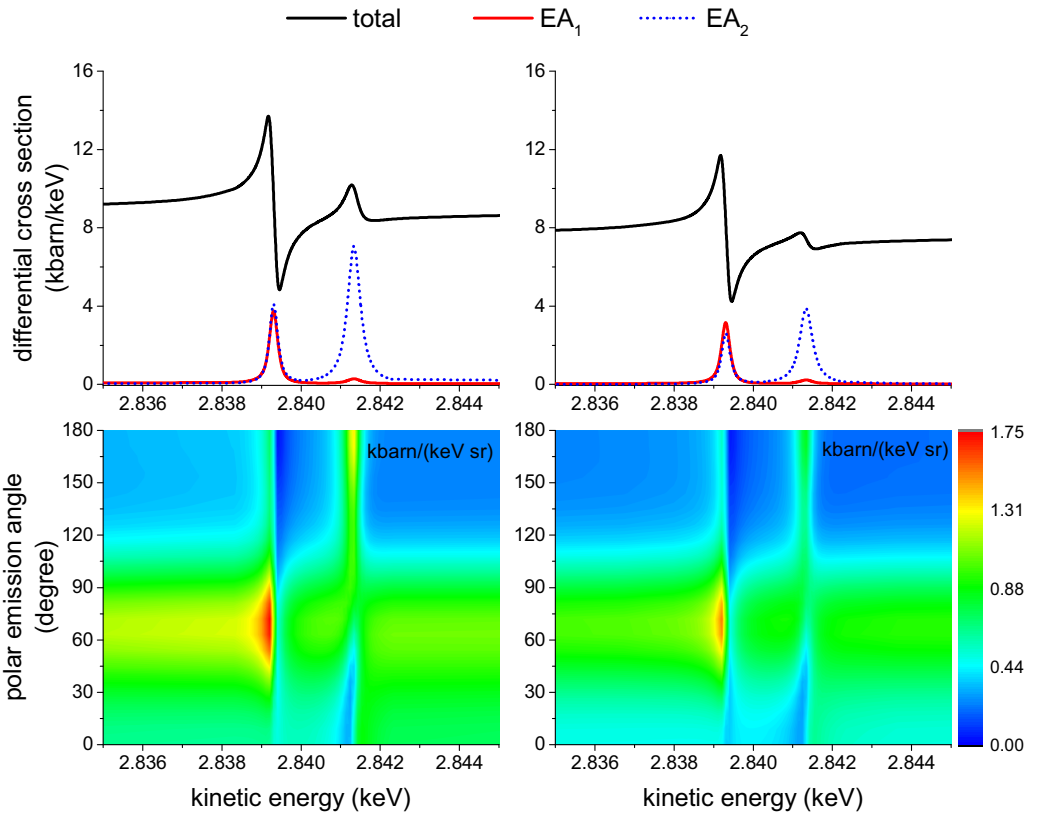

FIG. 6. Same as in Fig. 5 but for the energy range where only the $(2s2p_{3/2})_{J=1}$ and $(2p^2_{3/2})_{J=2}$ autoionizing states actively participate in the electron-loss process.

out of five angular dependences are qualitatively similar, showing a pronounced maximum at about 70° (the angular dependences corresponding to the other resonances present in Fig. 5 are qualitatively similar to these four). However, in the case of the $(2p^2_{3/2})_{J=2}$ state, the angular dependence is qualitatively different (we shall discuss the origin of this shape later).

In addition to autoionization, a doubly excited state can also decay via spontaneous radiative emission, which competes with the EA channel diminishing it. Therefore, it is of interest to compare the strength of the Auger decay with that of spontaneous radiative decay. This is done in Tables I and II, where the decay widths with the corresponding branching ratios are given.

Besides, in these tables, we present the resonant kinetic energies of the emitted electron ($E_{\rm res} = E_a - \varepsilon_{1s} - mc^2$, where $\varepsilon_{1s} = 505.5274$ keV for Ca and $\varepsilon_{1s} = 498.6036$ keV for Zn) and the binding energy of the autoionizing states ($E_a^{'} = E_a - 2mc^2$). These tables also show the contributions (ΔE) to the positions of resonances due to the radiative corrections (vacuum polarization and electron self-energy corrections). It is seen that for each resonance these corrections lead to the shift

TABLE I. Electron loss from Ca^{18+}. The positions of the resonances ($E_{\rm res} = E_a - \varepsilon_{1s} - m_e c^2$) with the radiative corrections (ΔE), the binding energies of the autoionizing states ($E_a^{'} = E_a - 2mc^2$), the radiative (Γ_r), Auger (Γ_a), and the total (Γ) widths of the corresponding autoionizing states, and the branching ratio (Γ_a/Γ).

	Autoionizing state	$E_{\rm res}$ (keV)	ΔE (eV)	$E_a^{'}$ (keV)	Γ_r (eV)	Γ_a (eV)	Γ (eV)	Γ_a/Γ
1	$(2s^2)_{J=0}$	2.7995	−1.3	−2.6704	0.026	0.235	0.26	0.90
2	$(2s2p_{1/2})_{J=0}$	2.8033	−1.4	−2.6667	0.066	0.015	0.08	0.18
3	$(2s2p_{1/2})_{J=1}$	2.8052	−1.4	−2.6647	0.066	0.013	0.08	0.16
4	$(2s2p_{3/2})_{J=2}$	2.8103	−1.4	−2.6597	0.066	0.010	0.08	0.13
5	$(2p^2_{1/2})_{J=0}$	2.8243	−1.6	−2.6456	0.128	<0.001	0.13	0.00
6	$(2p_{1/2}2p_{3/2})_{J=1}$	2.8271	−1.7	−2.6428	0.132	<0.001	0.13	0.00
7	$(2p_{1/2}2p_{3/2})_{J=2}$	2.8305	−1.6	−2.6394	0.132	0.027	0.16	0.17
8	$(2s2p_{3/2})_{J=1}$	2.8393	−1.4	−2.6306	0.066	0.131	0.20	0.66
9	$(2p^2_{3/2})_{J=2}$	2.8413	−1.6	−2.6286	0.132	0.219	0.35	0.63
10	$(2p^2_{3/2})_{J=0}$	2.8713	−1.5	−2.5986	0.108	0.015	0.12	0.13

TABLE II. Same as in Table I but for electron loss from Zn^{28+}.

	Autoionizing state	E_{res} (keV)	ΔE (eV)	E_a' (keV)	Γ_r (eV)	Γ_a (eV)	Γ (eV)	Γ_a/Γ
1	$(2s^2)_{J=0}$	6.2809	−4.9	−6.1081	0.136	0.238	0.38	0.63
2	$(2s2p_{1/2})_{J=0}$	6.2839	−5.4	−6.1052	0.331	0.024	0.35	0.07
3	$(2s2p_{1/2})_{J=1}$	6.2912	−5.4	−6.0979	0.331	0.024	0.36	0.07
4	$(2s2p_{3/2})_{J=2}$	6.3205	−5.4	−6.0685	0.331	0.011	0.34	0.03
5	$(2p_{1/2}^2)_{J=0}$	6.3251	−6.1	−6.0640	0.581	0.004	0.59	0.01
6	$(2p_{1/2}2p_{3/2})_{J=1}$	6.3459	−6.3	−6.0431	0.662	<0.001	0.66	0.00
7	$(2p_{1/2}2p_{3/2})_{J=2}$	6.3545	−6.3	−6.0345	0.662	0.109	0.77	0.14
8	$(2s2p_{3/2})_{J=1}$	6.3606	−5.4	−6.0285	0.331	0.124	0.45	0.28
9	$(2p_{3/2}^2)_{J=2}$	6.3897	−6.2	−5.9994	0.662	0.135	0.80	0.169
10	$(2p_{3/2}^2)_{J=0}$	6.4274	−6.1	−5.9616	0.604	0.028	0.63	0.04

of the position of the resonance, which substantially exceeds its total widths. Therefore, these corrections should be taken into account for an accurate description of the electron loss process. In contrast, the two-photon exchange yields corrections to the positions of the resonances which are of the same order of magnitude as the widths and thus much smaller then the radiative corrections.

The energy-angular distribution of the emitted electrons contains quite detailed information about the process. In particular, it follows from the results shown in the lower panels of Figs. 5 and 6 that the angular distribution of the emitted electrons at emission energies, which are sufficiently far from the resonance values, reaches a maximum at $\simeq 68^\circ$. However, in the vicinity of a resonance the shape of the angular distribution may be quite different for different resonances (see also Fig. 7). For instance, for electrons emitted in the energy range, where the $(2s2p_{3/2})_{J=1}$ autoionizing state participates in the ionization process, the shape of the angular distribution is rather similar to that at energies far from the resonances. This is in contrast with the angular distribution at energies, where the emission is strongly influenced by the presence of the $(2p_{3/2}^2)_{J=2}$ autoionizing state: Now the angular distribution reaches its maximum value at 180° (see also Fig. 7).

The fact that the electron prefers to be emitted mainly in the backward direction is quite interesting and it is worthwhile to get insight into the origin of such a behavior. In Fig. 8, we explore in detail the shape of the angular distribution at emission energy of 2.8413 keV corresponding to the position of the $(2p_{3/2}^2)_{J=2}$ resonance. Few main conclusions can be drawn from the figure. First, the total angular distribution

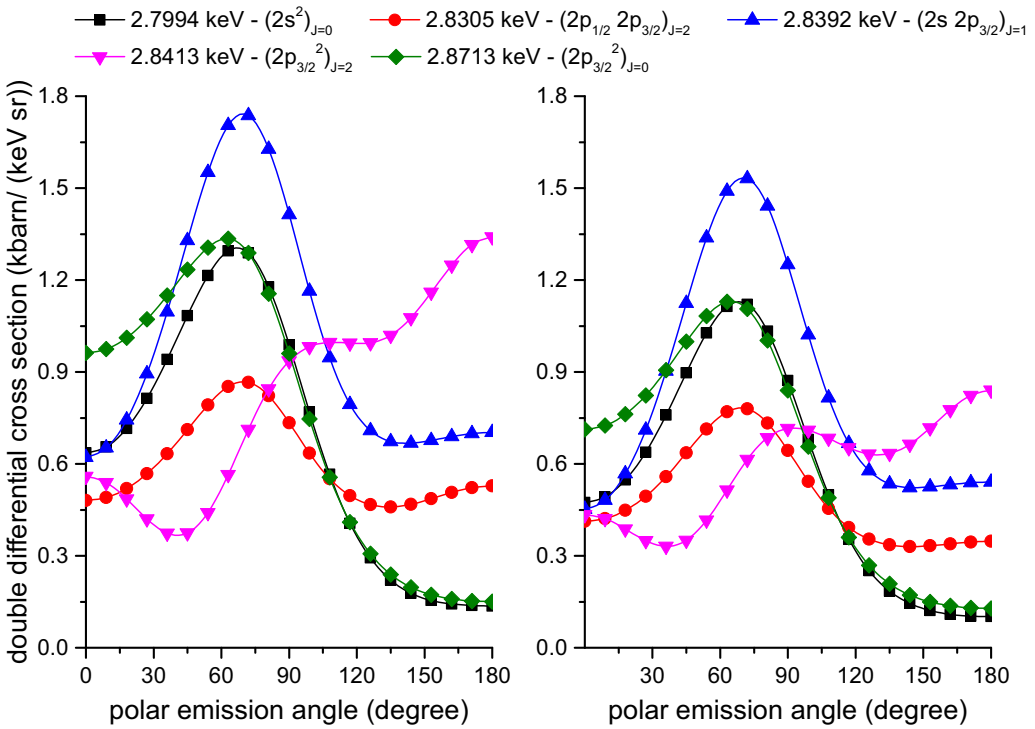

FIG. 7. Doubly differential cross section for the electron loss from Ca^{18+} $(1s^2)$ by the impact of 100 MeV/u bare neon nucleus (left) and 100 MeV/u neon atom (right). The cross section is given as a function of the polar emission angle for five resonant emission energies corresponding to the $(2s^2)_{J=0}$, $(2p_{1/2}2p_{3/2})_{J=2}$, $(2s2p_{3/2})_{J=1}$, $(2p_{3/2}^2)_{J=2}$, and $(2p_{3/2}^2)_{J=0}$ autoionizing states.

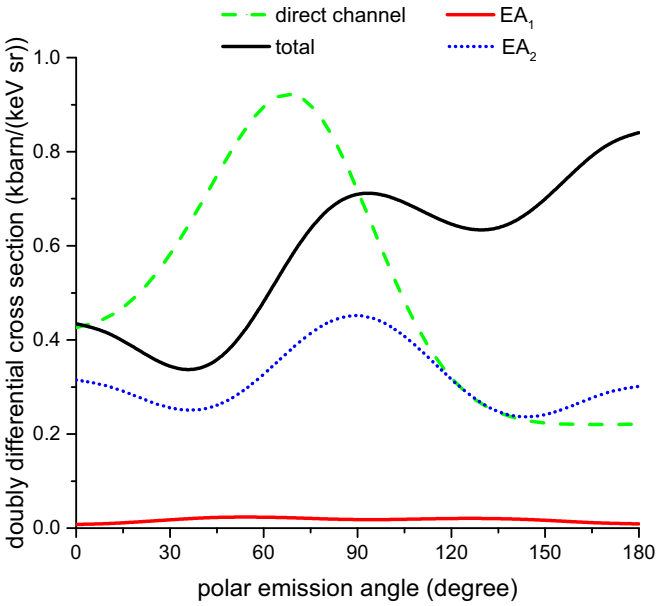

FIG. 8. Doubly differential cross section for the electron loss from Ca^{18+} $(1s^2)$ by the impact of 100 MeV/u neon atom. Emission energy is 2.8413 keV, which corresponds to a resonance with the $(2p^2_{3/2})_{J=2}$ autoionizing state.

has three maxima (at 0°, 90°, and 180°). Second, the EA_1 subchannel is of minor importance for all emission angles, as expected. Third, the direct channel leads to electron emission mainly in the forward semisphere. Fourth, the EA_2 subchannel leads to an almost symmetric angular distribution which peaks at 90° and has two more maxima at 0° and 180°. We thus see that the maximum at 180° in the total angular distribution is caused by constructive interference between the direct channel and the EA_2.

Cross sections for electron loss from Ca^{18+} in collisions with neutral neon at an impact energy of 100 MeV/u are displayed in the right columns of Figs. 5–7. By comparing them with the corresponding results for collisions with equivelocity bare neon nuclei, we see that the presence of atomic electrons has overall a rather weak effect on the electron loss process. The reason for this is that the electrons in the HCI are tightly bound and, as a result, the loss process involves momenta transfers which are large on the typical atomic scale of neon that makes the effective charge of the atom $Z_A(\mathbf{Q})$, given by Eq. (20), to be approximately equal to the charge of the unscreened atomic nucleus for the most important range of the momentum transfers contributing to the loss process.

One could add that the origin of the weakness of the screening effect in collisions with HCI can be viewed also from a different perspective. Namely, due to the small size of the ground state of electrons tightly bound in the HCI (and because of not very large impact velocity), the loss process takes place mainly in collisions with impact parameters much smaller than the size of the atom. Therefore, only a small fraction of the atomic electron cloud can stay between the electrons of the HCI and the nucleus of the atom that weakens the screening effect.

In Figs. 9–11, we show results for the electron loss from $Zn^{28+}(1s^2)$ in collisions with neon at an impact energy of

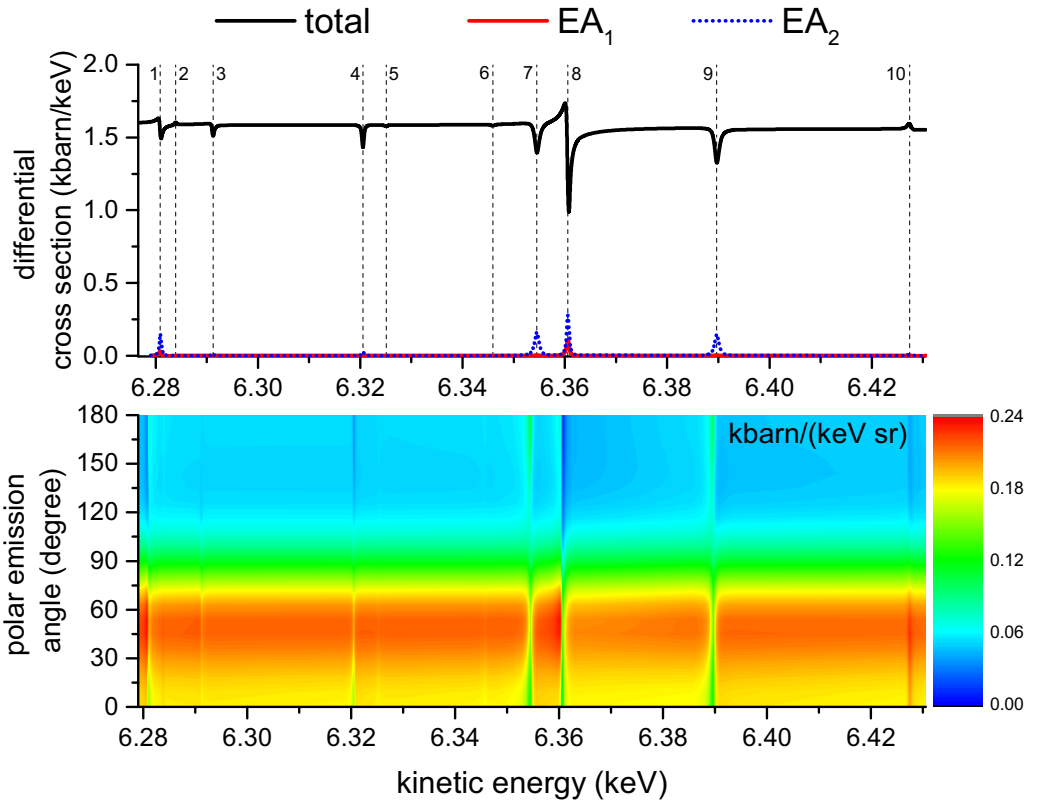

FIG. 9. Cross sections for single-electron loss from Zn^{28+} $(1s^2)$ by the impact of 100 MeV/u bare neon nucleus. The upper and lower panels present the energy and energy-angular distributions, respectively, of the emitted electron. The cross sections are given in the rest frame of the HCI. The numbered vertical lines refer to resonances arising due to the autoionizing states listed in Table II.

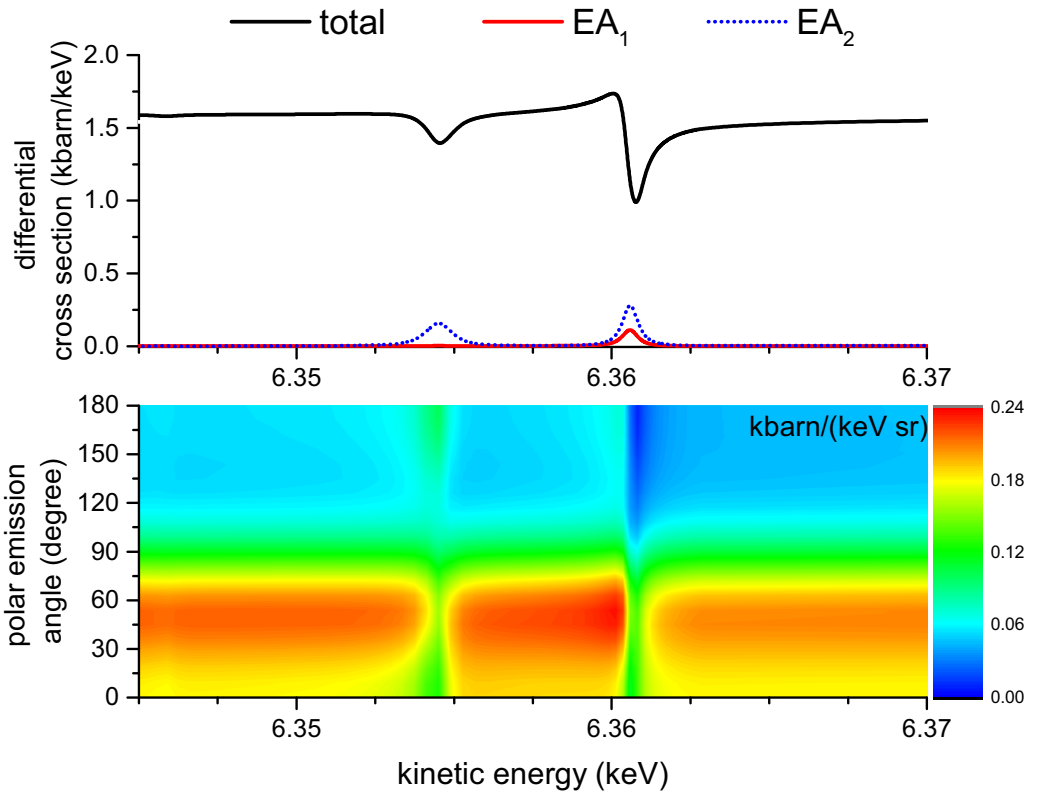

FIG. 10. Same as in Fig. 9 but for the energy range where only the $(2p_{1/2}2p_{3/2})_{J=2}$ and $(2s2p_{3/2})_{J=1}$ autoionizing states actively participate in the electron loss process.

100 MeV/u. Since the electrons in $Zn^{28+}(1s^2)$ are much more tightly bound than those in $Ca^{18+}(1s^2)$, the screening effect of atomic electrons in the electron loss from Zn^{28+} in collision with neutral neon atoms is even weaker than that for the electron loss from $Ca^{18+}(1s^2)$. Therefore, in the case of electron loss from $Zn^{28+}(1s^2)$, we present results only for collisions with Ne^{10+}.

Similar to the electron loss from Ca^{18+}, we observe in Figs. 9 and 10 that the energy spectrum of the emitted electrons contains sharp maxima and minima appearing due to the EA channel and its interference with the direct channel of electron loss. Now, however, they are less pronounced, which is related to the diminishing role of the EA channel in electron loss with increase in the atomic number of the HCI. The diminishing role of the EA can be also unveiled by considering the angular spectra (see Fig. 11), where now all angular distributions, being dominated by the direct channel, look qualitatively similar.

One can show that the EA_2-to-EA_1 amplitude ratio roughly scales as $\frac{\alpha Z_A Z_I}{v}$ [31]. Therefore, the contribution of the EA_2 subchannel to the EA becomes more important when Z_I and/or Z_A/v increase. In particular, the increase with Z_I follows from the comparison of the results shown in Figs. 5, 6 and the results shown in Figs. 9, 10. Since the use of the perturbation theory is limited to $\alpha Z_A/v \ll 1$, it is obvious that for fast collisions the high visibility of the EA_2 subchannel in the EA is a *qualitative feature* inherent to electron loss from (the ground state of) heliumlike HCIs.

By comparing the results for electron loss from Ca^{18+} and Zn^{28+}, we also see that the shape of the angular emission spectra noticeably depends on the atomic number of the HCI. This dependence is caused not only by the fact that the relative importance of the direct and EA channels is a function of Z_I

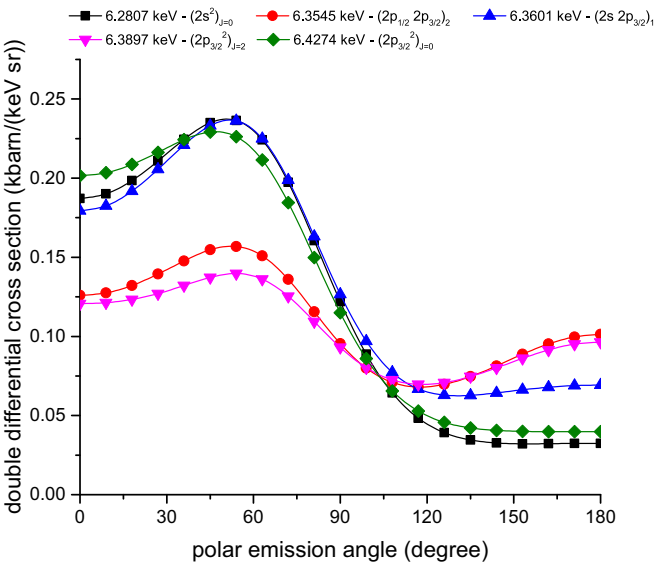

FIG. 11. Doubly differential cross section for the electron loss from Zn^{28+} $(1s^2)$ by the impact of 100-MeV/u neon atom (right). The cross section is given as a function of the polar emission angle for five resonant emission energies corresponding to the $(2s^2)_{J=0}$, $(2p_{1/2}2p_{3/2})_{J=2}$, $(2s2p_{3/2})_{J=1}$, $(2p^2_{3/2})_{J=2}$, and $(2p^2_{3/2})_{J=0}$ autoionizing states.

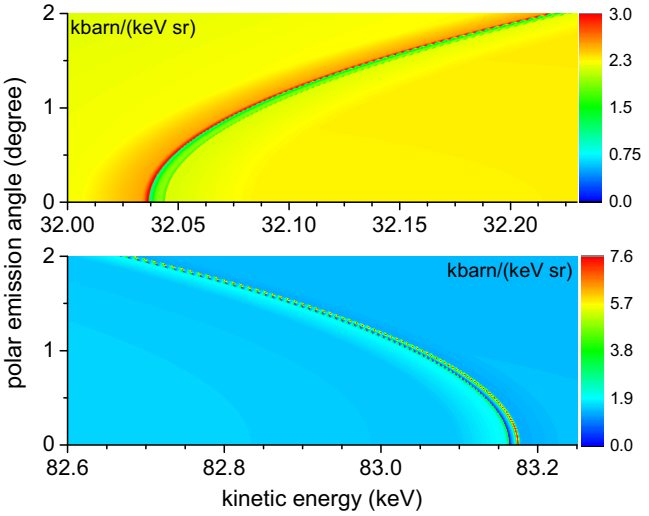

FIG. 12. Doubly differential cross section for single-electron loss from 100 MeV/u Ca^{18+} $(1s^2)$ in collision with neon given in the rest frame of neon. Resonant energy-angle region corresponds to the $(2s2p_{3/2})_{J=1}$ and $(2p^2_{3/2})_{J=2}$ autoionizing states.

but also by the Z_I dependence of the ratio between the typical momentum transfer to the HCI in the collision and the typical orbiting electron momenta in the HCI. Indeed, the former and the latter scale with Z_I approximately as $\sim Z_I^2$ and $\sim Z_I$, respectively. The growth of the ratio leads to the increase of the effective number of the partial waves contributing to the state of the emitted electron that changes the shape of the emission pattern. Besides, as calculations show, the effective magnitude of the transverse component $Q_\perp$ of the momentum transfer $\mathbf{Q}$ increases with Z_I somewhat less rapidly than its longitudinal component $Q_{\min}$ ($Q_{\min} \sim Z_I^2$). This makes the orientation of $\mathbf{Q}$ effectively Z_I dependent. Since the relative populations of the magnetic sublevels of the autoionizing and continuum states in the collision depend on the orientation of $\mathbf{Q}$ with respect to the quantization axis, the relative populations of these sublevels for Ca^{18+} and Zn^{28+} turn out to be different, which leads to changes in the emission pattern.

B. Spectra of electrons emitted from a moving HCI

Up to now, we have discussed the electron emission spectra by considering them in the rest frame of the HCI. Such a theoretical discussion would be directly relevant to a possible experimental exploration of electron loss if the ion rests in the laboratory frame.

However, a more realistic is a situation in which a quickly moving HSI loses an electron in collision with an atom (or with an effectively bare atomic nucleus). Such a situation can be experimentally realized in accelerators of heavy ions when a beam of fast heliumlike highly charged projectiles penetrates a gas target which rests in the laboratory frame. Therefore, in Fig. 12 we display results for electron emission from a moving HCI calculated for the laboratory frame. These electrons are emitted from $Ca^{18+}(1s^2)$ ions, which move in the laboratory frame with an energy of 100 MeV/u, colliding with a neon target.

In this figure, we focus on very small emission angles ($\vartheta \leqslant 2^\circ$) which are relevant for the electron spectrometer currently functioning at the GSI (Darmstadt, Germany). It can measure spectra of high-energy electrons which move within an angle of about 2° with respect to the projectile velocity (see, e.g., Ref. [32]). In order not to overload the figure, for these angles we consider just those ranges of electron emission energies for which only the $(2s2p_{3/2})_{J=1}$ and $(2p^2_{3/2})_{J=2}$ autoionizing states are involved. One can conclude from the figure that the signatures of the EA channel in electron loss are clearly seen also in the frame where the HCI moves.

Since it is much simpler to ionize a neutral atom than to produce electron loss from a HCI, it is obvious that in fast collisions between a heliumlike HCI and a neutral atom the overwhelming majority of the emitted electrons will originate from the atom. Therefore, for a possible experimental verification of the results presented in this paper, it is very important to find out whether the spectra of electrons shown in Fig. 12 will not be masked by electron emission from the atoms. In order to answer this point, we have estimated cross sections for ionization of neon atoms in collisions with 100 MeV/u Ca^{18+}.

We evaluated the differential cross section for single ionization of neon in collision with 100 MeV/u Ca^{18+} as follows. We used the first-order perturbation theory in the interaction between neon and Ca^{18+} in order to calculate the differential cross sections for removal of single electron from the K and L shells of neon, assuming that the corresponding electrons can be described as a moving in the Coulomb field with an effective charge ($Z_{\rm eff} = 9.7$ for the K shell electrons and $Z_{\rm eff} = 5.85$ for the L shell electrons; see Ref. [33]). The resulting cross section for single ionization was obtained by taking into account the corresponding contributions from each of the electrons of Ne. According to this simple estimate, the cross section for ionization of neon has maximum of 0.007 kb/(keV sr) and 0.001 kb/(keV sr) in the upper and lower panels, respectively, of Fig. 12. Although these numbers are obtained using the approach, which is obviously not very accurate, they are so much smaller than the cross section for electron loss from Ca^{18+} that one can conclude that the contribution of neon ionization to the energy-angle range shown in Fig. 12 can be safely neglected.

C. Electron loss by charged particle impact versus electron loss by photoabsorption

The relationship between the processes of ionization (electron loss) by photoabsorption and by the impact of a charged particle is of fundamental importance since its consideration offers a deeper insight into subtle details of the response of atoms, ions, and molecules to the action of electromagnetic fields. As known, these two types of ionization (electron loss) in general qualitatively differ from each other.

Here we shall very briefly discuss this relationship in cases when autoionization is involved by considering that only one photon participates in the process of photoelectron loss and also that electron loss by charged particle impact proceeds via just a single interaction between the colliding particles (the exchange of one virtual photon). Under such conditions, any difference between these two electron-loss processes should be fully attributed to the difference between the properties (momentum and polarization) of a real and virtual photon.

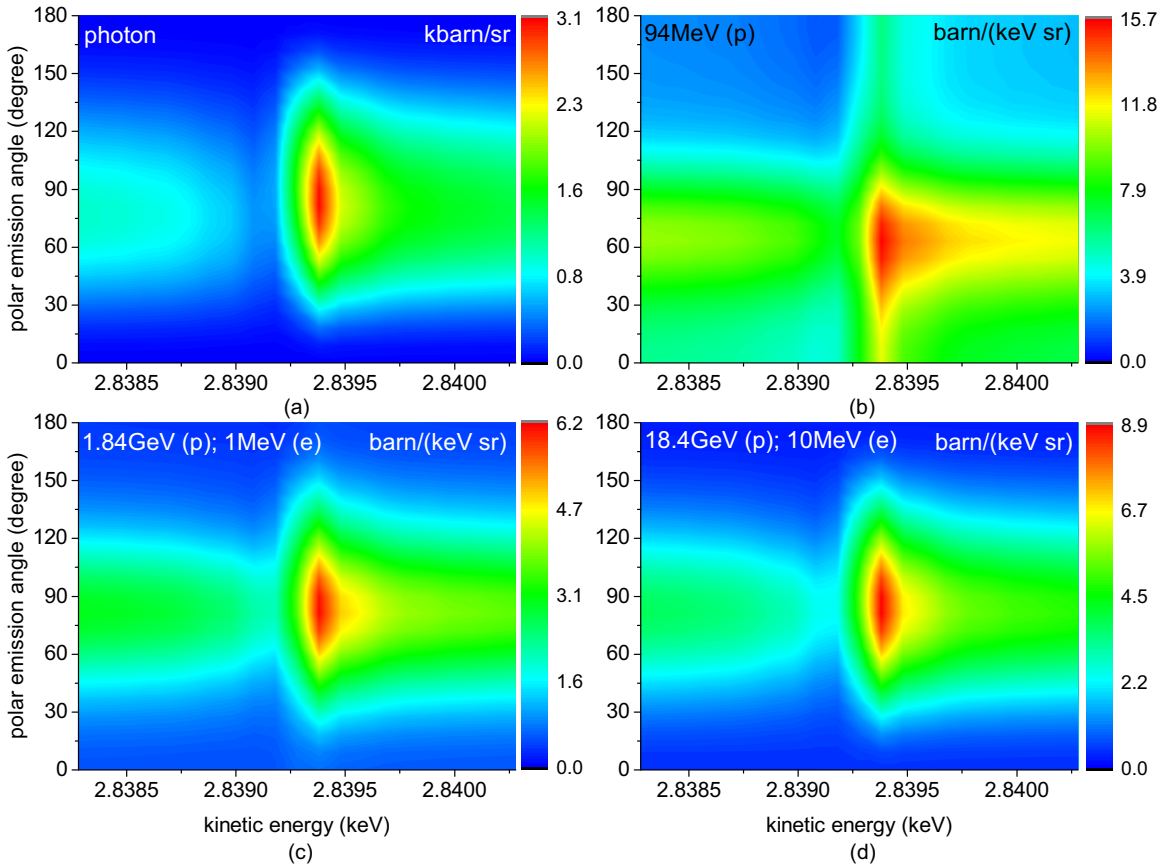

FIG. 13. The comparison of electron loss from $Ca^{18+}(1s^2)$ via photoabsorption (a) and by the impact of a charged particle [proton, (b)–(d); electron, (c) and (d)]. The emission energy range corresponds to the participation of the $(2s2p_{3/2})_{J=1}$ autoionizing state. The spectra of emitted electrons are given in the rest frame of the HCI in which both the incident photon and the charged particle move along the z axis ($\vartheta = 0^\circ$).

In the case of ionization of light atomic systems, in which the electron motion is nonrelativistic, the differences between these properties were discussed in detail in Ref. [34]. There, in particular, it was shown that a virtual photon representing the field of a charged particle becomes almost real if the following conditions are fulfilled:

$$\frac{q_{\min}}{\gamma^2} \ll q_\perp \ll q_{\min}. \tag{22}$$

It can be easily shown that the same holds true also for electron loss from tightly bound systems, like HCIs, where the electron motion is already relativistic.

The correspondence between electron loss by photoabsorption and by the impact of a charged particle (proton, electron) is illustrated in Fig. 13, where the impact energy of the incident proton ranges from a modest relativistic value of ≈94MeV ($\gamma = 1.1$) to extreme relativistic energies (and the corresponding energies of an equivelocity electron except the lowest one, which cannot be treated in the semiclassical approximation). It is seen that the shapes of the emission pattern in electron loss by photoabsorption and by the charged particle impact can be very similar, provided the energy of the incident particle is high enough.

IV. SUMMARY

We have considered electron loss from the ground state of heliumlike highly charged ions in fast collisions with atomic particles. In this consideration, we supposed that the field of the atomic particle in the collision represents a relatively weak perturbation for electrons of the HCI. We have performed calculations for the energy and energy-angular distributions of electrons emitted from $Ca^{18+}(1s^2)$ and $Zn^{28+}(1s^2)$ in collisions with neon at 100-MeV/u impact energy.

Electron loss in general proceeds via two different pathways which can (partially) interfere. In one of them, an electron of the ion undergoes a direct transition from the initial state to the continuum. For highly charged ions, this direct channel is essentially a single-electron transition. In the other—the EA channel—the ion is excited in the collision into an autoionizing state which then Auger decays. The main focus of our study was on the role of this channel. In particular, its presence leads to the appearance of sharp structures in the energy distribution of the emitted electrons. The EA may also noticeably influence the angular distributions of the emission in the vicinity of resonances.

We have shown that for electron loss from the ground state of heliumlike HCI there are two main subchannels contributing to the EA and they both have been explored in our study. In one of them (EA_1), an autoionizing state is excited via just a single interaction between the electrons of the HCI and the atomic particle. Within this subchannel, in order to excite an autoionizing state, the interaction between the electrons of the HCI is absolutely necessary. Since Auger decay also proceeds

via this interaction, the EA_1 represents a highly correlated subchannel of electron loss.

In the other EA's subchannel (EA_2), the atomic particle interacts with both electrons of the HCI and the excitation of an autoionizing state can now take place without electron correlations. Since the relative strength of the electron-electron interaction in the HCI decreases when the atomic number of the ion increases [31], the role of this less correlated subchannel in the EA increases, with Z_I becoming important even in fast collisions where the field of the incident particle represents an already weak perturbation for the electrons of the HCI.

We have found that both EA_1 and EA_2 substantially interfere with the direct channel of electron loss. However, they practically do not interfere with each other.

Our consideration has also shown that the account of QED corrections is important for an accurate description of electron loss even from relatively light heliumlike HCIs like, for instance, Ca^{18+}.

Experiments on electron loss from heliumlike highly charged ions in fast collisions with atoms seem to be feasible at the GSI (Darmstadt, Germany).

ACKNOWLEDGMENTS

We are grateful to C. Müller for useful discussions. The work of K.N.L. and O.Y. A. presented in Sec. II A was supported by the Russian Science Foundation under Grant No. 17-12-01035. The work of K.N.L. (except the part presented in Sec. II A) was also supported by RFBR Grant No. 16-32-00620 and by the German-Russian Interdisciplinary Science Center (G-RISC) funded by the German Federal Foreign Office via the German Academic Exchange Service (DAAD).

APPENDIX: AUGER PART OF TWO-PHOTON EXCHANGE CORRECTION

Within the framework of QED, the Auger widths are obtained from the imaginary part of the two-photon exchange corrections (the Auger part of the two-photon exchange correction). In the case of heavy HCIs, the Auger widths are usually much smaller than the radiative widths and are simply neglected. However, in the case of relatively light HCI (e.g., Ca^{18+} and Zn^{28+}), the Auger widths become of importance and have to be taken into account. Correspondingly, the LPA [20] has to be generalized in order to account for the Auger widths.

In the framework of the LPA, the expression for two-photon exchange correction is derived in Ref. [20] [see Eqs. (294) and (298)]. In these expressions, the double summation (n_1, n_2) over the complete Dirac spectrum takes place. In order to obtain the Auger widths, we have to evaluate the imaginary part of those terms in this double summation for which (n_1,n_2) are equal to ($1s$,e^-), where e^- represents the corresponding continuum state of the Dirac spectrum with energy $\varepsilon = \varepsilon_{u_1} + \varepsilon_{u_2} - \varepsilon_{1s}$. After a relatively simple calculation, the imaginary part of these terms can be written as

$$\begin{aligned}\Delta V^{(a)}_{u_1u_2d_1d_2} = &-\pi i\left[I\left(\left|\varepsilon_{n_2}-\varepsilon_{u_2}\right|\right)\right]_{u_1u_2n_1n_2}\\ &\times\left[I\left(\left|\varepsilon_{n_2}-\varepsilon_{d_2}\right|\right)\right]_{n_1n_2d_1d_2}\\ &-\pi i\left[I\left(\left|\varepsilon_{n_1}-\varepsilon_{u_2}\right|\right)\right]_{u_1u_2n_2n_1}\\ &\times\left[I\left(\left|\varepsilon_{n_1}-\varepsilon_{d_2}\right|\right)\right]_{n_2n_1d_1d_2},\end{aligned} \tag{A1}$$

where d_i, u_i, and n_i denote one-electron states with energies ε_{d_i}, ε_{u_i}, and ε_{n_i}, respectively ($i = 1,2$). Autoionizing states are composed from these excited one-electron states: (d_1,d_2) and (u_1,u_2), e.g., ($2s2s$), ($2s2p$) ($2p2p$).

In Eq. (A1), the quantity $[I(|\Omega|)]_{f_1f_2n_1n_2}$ denotes the matrix element of one-photon exchange

$$\begin{aligned}[I(\Omega)]_{n_1n_2n_3n_4} = &\int d^3\mathbf{r}_1 d^3\mathbf{r}_2\, \psi_{n_1}(\boldsymbol{r}_1)\psi_{n_2}(\boldsymbol{r}_2)(-i\alpha)\\ &\times\gamma^{\mu_1}\gamma^{\mu_2} I_{\mu_1\mu_2}(\Omega,|\boldsymbol{r}_1-\boldsymbol{r}_2|)\psi_{n_3}(\boldsymbol{r}_1)\psi_{n_4}(\boldsymbol{r}_2),\end{aligned} \tag{A2}$$

where ψ_{n_i} is a solution of Dirac equation corresponding to the set of quantum numbers $n_i = (n_i, j_i, l_i, m_i)$ ($i = 1,2,3,4$), γ^μ are the gamma matrices ($\mu = 0,1,2,3$), and $I(\Omega,|\boldsymbol{r}_1-\boldsymbol{r}_2|)$ is the photon propagator [20].

The application of the nondegenerative perturbation theory would lead to the following expression for the Auger width Γ_a:

$$\Gamma_a = 2i\,\Delta V^{(a)}_{n_1n_2n_1n_2}. \tag{A3}$$

However, in our case the two-electron configurations are strongly mixed because of (quasi)degeneracy. Correspondingly, in our calculation we have to employ the degenerative perturbation theory and the Auger width appears as a correction to the total width arising from taking into account the matrix $\Delta V^{(a)}$ [see Eq. (A1)]. It is important to note that in order to obtain accurate results for the Auger widths, not only diagonal but also nondiagonal elements of this matrix have to be taken into account. The Auger widths, which we calculate within the LPA, are in good agreement with the results obtained in Refs. [35,36].

[1] R. P. Madden and K. Codling, Astrophys. J. **141**, 364 (1965).
[2] S. Ormonde, W. Whitaker, and L. Lipsky, Phys. Rev. Lett. **19**, 1161 (1967).
[3] A. Raeker, K. Bartschat, and R. H. G. Reid, J. Phys. B **27**, 3129 (1994).
[4] A. Müller, G. Hofmann, B. Weissbecker, M. Stenke, K. Tinschert, M. Wagner, and E. Salzborn, Phys. Rev. Lett. **63**, 758 (1989).
[5] K. T. Dolder and B. Peart, Rep. Prog. Phys. **39**, 693 (1976).
[6] M. S. Pindzola, D. C. Griffin, and C. Bottcher, Phys. Rev. A **25**, 211 (1982).
[7] B. Peart, J. G. Stevenson, and K. T. Dolder, J. Phys. B **6**, 146 (1973).
[8] R. K. Feeney, J. W. Hooper, and M. T. Elford, Phys. Rev. A **6**, 1469 (1972).
[9] D. H. Crandall, R. A. Phaneuf, B. E. Hasselquist, and D. C. Gregory, J. Phys. B **12**, L249 (1979).
[10] R. A. Falk, G. H. Dunn, D. C. Griffin, C. Bottcher, D. C. Gregory, D. H. Crandall, and M. S. Pindzola, Phys. Rev. Lett. **47**, 494 (1981).
[11] A. Borovik, Jr., M. F. Gharaibeh, P. M. Hillenbrand, S. Schippers, and A. Müller, J. Phys. B **46**, 175201 (2013).

[12] D. C. Griffin, C. Bottcher, M. S. Pindzola, S. M. Younger, D. C. Gregory, and D. H. Crandall, Phys. Rev. A **29**, 1729 (1984).
[13] A. Borovik, Jr., C. Brandau, J. Jacobi, S. Schippers, and A. Müller, J. Phys. B **44**, 205205 (2011).
[14] S. S. Tayal and R. J. W. Henry, Phys. Rev. A **44**, 2955 (1991).
[15] H. J. W. Henry, J. Phys. B **12**, L309 (1979).
[16] C. P. Ballance, S. D. Loch, J. A. Ludlow, S. A. Abdel-Naby, and M. S. Pindzola, Phys. Rev. A **84**, 062713 (2011).
[17] M. H. Chen and K. J. Reed, Phys. Rev. A **48**, 1129 (1993).
[18] S. Fritzsche, A. Surzhykov, A. Gumberidze, and T. Stöhlker, New J. Phys. **14**, 083018 (2012).
[19] A. Müller, *Electron-Ion Collisions: Fundamental Processes in the Focus of Applied Research* (Elsevier, Amsterdam, 2008).
[20] O. Y. Andreev, L. N. Labzowsky, G. Plunien, and D. A. Solovyev, Phys. Rep. **455**, 135 (2008).
[21] O. Y. Andreev, L. N. Labzowsky, and A. V. Prigorovsky, Phys. Rev. A **80**, 042514 (2009).
[22] It is worth noting that whereas the graph in Fig. 2(a) does not contribute to the EA channel, the graphs in Figs. 2(b)–2(e) include also some corrections to the direct channel.
[23] A. I. Akhiezer and V. B. Berestetskii, *Quantum Electrodynamics* (Wiley Interscience, New York, 1965).
[24] N. Stolterfoht, R. D. DuBois, and R. D. Rivarola, *Electron Emission in Heavy Ion-Atom Collisions* (Springer, Berlin, 1997).
[25] J. H. McGuire, *Electron Correlation Dynamics in Atomic Collisions* (Cambridge University Press, Cambridge, UK, 1997).
[26] A. B. Voitkiv and J. Ullrich, *Relativistic Collisions of Structured Atomic Particles* (Springer, Berlin, 2008).
[27] Since the effect of the atomic electrons in the inelastic atomic mode is opposite to that in the elastic one, the inelastic mode is often called antiscreening; see, e.g., Refs. [24–26].
[28] G. Moliére, Z. Naturforschg. **2a**, 133 (1947).
[29] F. Salvat, J. D. Marťinez, R. Mayol, and J. Parellada, Phys. Rev. A **36**, 467 (1987).
[30] U. Fano, Phys. Rev. **124**, 1866 (1961).
[31] This is valid if the Breit part of the electron-electron interaction still plays a minor role compared to Coulomb part.
[32] P.-M. Hillenbrand, S. Hagmann, A. B. Voitkiv, B. Najjari *et al.*, Phys. Rev. A **90**, 042713 (2014).
[33] M. G. Veselov, and L. N. Labzowsky, *Teoriya Atoma. Stroenie Elektronnyh Obolochek.* [*Theory of Atoms: The Structure of Electron Shells*] (Nauka, Moscow, 1986).
[34] A. B. Voitkiv and J. Ullrich, J. Phys. B **34**, 4513 (2001).
[35] L. N. Labzowsky, *Teoriya Atoma. Kvantovaya Elektrodinamika Elektronnyh Obolochek i Processy Izlucheniya* [*Theory of Atoms: Quantum Electrodynamics of the Electron Shells and the Processes of Radiation*] (Nauka, Moscow, 1996).
[36] P. Zimmerer, N. Grün, and W. Scheid, Phys. Lett. A **148**, 457 (1990).